Study of the $^{11}C(p,\gamma)$ reaction via the indirect $d(^{11}C,^{12}N)n$ transfer reaction

D.W. Lee,[1,*] J. Powell,[1] K. Perajarvi,[1,†] F.Q. Guo,[1,2,‡] D.M. Moltz,[2] and Joseph Cerny [1,2]

[1] Nuclear Science Division, Lawrence Berkeley National Laboratory, Berkeley, California 94720, USA
[2] Department of Chemistry, University of California, Berkeley, California 94720, USA

PACS number(s): 21.10.Jx, 25.40.Lw, 25.60.Je, 26.30.+k

The $^{11}C(p,\gamma)^{12}N$ reaction is expected to be an important branch point in supermassive low-metallicity stars because it could produce CNO seed nuclei before the traditional triple-alpha process turns on. In the present work, the $d(^{11}C, ^{12}N)n$ transfer reaction was employed to evaluate this reaction using a radioactive ion beam of 150 MeV ^{11}C with 6×10^5 ions/s on target from the BEARS project at the 88-inch cyclotron at Lawrence Berkeley National Laboratory. Excellent agreement was obtained between the experimental cross sections ($\theta_{c.m.}$=10.9° to 71.5°) and DWBA calculations. The asymptotic normalization coefficient was deduced to be $(C_{eff}^{12N})^2 = (C_{p1/2}^{12N})^2 + (C_{p3/2}^{12N})^2 = 1.83 \pm 0.27\, fm^{-1}$.

* dwlee@lbl.gov
† Present address: Radiation and Nuclear Safety Authority, Helsinki, Finland
‡ Present address : Yale University, New Haven, Connecticut, USA

I. INTRODUCTION

When a massive star consumes all its pp-chain fuel, and gravitational contraction becomes more dominant than outward thermal expansion, the triple-α particle process producing ^{12}C nuclei turns on too late to prevent the star from collapsing into a black hole. Fuller et.al. [Fu86] showed that the existence of even a small amount of CNO seed nuclei prior to the helium burning stage could slow down the process of collapse and change the destiny of the star. Wiescher et.al. [Wi89] suggested several reaction sequences ("the hot pp-chain"), which lead to the formation of ^{12}C, instead of the traditional 3α process. These include the sequences $^{7}Be(\alpha,\gamma)^{11}C(p,\gamma)^{12}N(e^{+}\nu)^{12}C$ and $^{8}B(\alpha,p)^{11}C(p,\gamma)^{12}N(e^{+}\nu)^{12}C$. Sequences which involve ^{11}C production could be more efficient ways for ^{12}C formation, bypassing the slow 3α reaction, so that the $^{11}C(p,\gamma)^{12}N$ reaction rate and its astrophysical S-factor become of interest.

A GANIL experiment using Coulomb breakup of ^{12}N has shown that direct capture of protons by ^{11}C nuclei to the ground state is the most important production mechanism of ^{12}N in the temperature region below $0.3T_9$ [Le95]. At higher temperature, proton capture through the first two resonance states in ^{12}N becomes more significant. The $^{11}C(p,\gamma)$ radiative capture reaction scheme is shown in Fig. 1. The Asymptotic Normalization Coefficient (ANC) method [Mu01, Ga02, Mu06] for determining the direct capture component has been employed using the $^{14}N(^{11}C,^{12}N)^{13}C$ reaction at Texas A&M [Ta03] and the $d(^{11}C,^{12}N)n$ reaction at Beijing [Li03]. These experiments agreed on two conclusions: 1) the astrophysical S-factor and reaction rate based on the extracted ANC values are much higher than were theoretically predicted, and 2) the direct proton capture of ^{11}C leading to the ^{12}N ground state is more important than resonance capture in the

temperature region of interest (< $0.3T_9$). However, the extracted ANC values in these two experiment differ from one another by 50%, and the d(^{11}C,^{12}N)n experiment was limited by low statistics, so that its experimental ANC value, $(C_{eff})^2 = 2.86 \pm 0.91 fm^{-1}$, has a large uncertainty [Li03].

II. EXPERIMENT

The BEARS facility (Berkeley Experiments with Accelerated Radioactive Species) at Lawrence Berkeley National Laboratory's (LBNL's) 88-inch cyclotron provides several proton-rich radioactive ion beams for studies of exotic nuclei and nuclear astrophysics (^{14}O [Gu05], ^{11}C [Jo00], and ^{15}O [Le07]). Among its radioactive ion beams, ^{11}C ($T_{1/2}$ = 20 min.) has been used to investigate several nuclear reactions. ^{11}C is produced via ^{14}N(p,α) reactions by bombarding 40 μA of 10 MeV protons from LBNL's Life Sciences Division's medical cyclotron onto a nitrogen gas target; ^{11}C is extracted from the target in the form of carbon dioxide ($^{11}CO_2$) and transported 350 meters via a capillary line to the 88-inch cyclotron for injection into its Advanced Electron Cyclotron Resonance ion source [Po00, Po03].

In order to deliver the 150 MeV $^{11}C^{4+}$ beam to Cave 4A for the experiment, a 300 MeV $^{22}Ne^{8+}$ pilot beam was first used to tune the cyclotron and beam line optics. Next, the beam optics was set to focus a weak $^{11}B^{4+}$ beam on target, whose cyclotron frequency is very close to that of $^{11}C^{4+}$ (the cyclotron frequency difference is only 1.4 kHz). Finally, a $^{11}C^{4+}$ beam was accelerated and stripped to its 6+ charge state by using an upstream stripper foil (204 μg/cm^2 Al foil) and bending magnet combination in order to eliminate ^{11}B contamination.

Figure 2 (a) shows the experimental setup for the d(^{11}C,^{12}N)n reaction. The focused ^{11}C beam passed through a series of Ta collimators and impinged on 2.22 mg/cm^2 CD_2 target (deuterated polyethylene). Emitted ^{12}N nuclei from the d(^{11}C,^{12}N)n reaction were measured in a detector telescope, located 65 cm away from the target. This detector telescope was composed of rectangular 7-strip ΔE (60 μm thick) and E (1 mm thick) silicon detectors with a cooling system. A trapezoidal shaped collimator in front of the detector telescope was necessary to define the angles of each detector strip as shown in Fig. 2 (b). As a result, it was possible for us to attempt to measure the forward ($0° < \theta_{c.m.} < 90°$) and backward ($90° < \theta_{c.m.} < 180°$) ^{12}N peaks at seven different laboratory angles. The laboratory angles of the seven strips were 1.2, 2.0, 2.8, 3.7, 4.5, 5.3, and 6.2 degrees, from strip 1 to strip 7, respectively: these laboratory angles correspond to the center of mass (c.m.) angles of 10.9 (119.0), 18.9 (134.1), 27.1 (143.5), 35.9 (151.4), 45.4 (158.5), 56.5 (165.1), and 71.5 (171.4) degrees for the forward (backward) peaks, respectively.

An additional single Si detector (1 mm thick) was located at 0° to determine the ^{11}C beam intensity, calibrate a Faraday cup for use during the main experiment, and measure the beam quality and energy spread. The average beam intensity of the 150 MeV $^{11}C^{6+}$ beam on target was about 6×10^5 ions/sec. A typical ^{11}C beam energy spread without a target was measured to be 1.18 MeV FWHM.

A typical two-dimensional ΔE-E_{total} spectrum from the d(^{11}C,^{12}N)n reaction is shown in Fig. 3 (a), and a $^{12}N_{g.s.}$ forward peak is clearly observed above the scattered ^{11}C. Figure 3 (b) shows the gated ^{12}N spectrum. In order to calibrate the detection system, the d(^{12}C,^{13}N)n experiment was also performed with the same setup. The d(^{12}C,^{13}N)n angular distribution is shown in Fig. 4. This reaction also allowed us to compare our experimental

results with the $^{12}C(d,n)^{13}N_{g.s.}$ reaction at 25 MeV [Ka86]: they used a 25 MeV deuteron beam on a ^{12}C target ($E_{c.m.}$= 21.41 MeV) in conventional kinematics, which is nearly equivalent to our 150 MeV ^{12}C beam on a deuteron target ($E_{c.m.}$= 21.56 MeV) in inverse kinematics. Our cross section turned out to be somewhat lower than that of the previous study, but the difference is less than 3% at the smallest c.m. angle ($\theta_{c.m.} = 10.9^{\circ}$). Three theoretical angular distributions are also shown in Fig. 4, as discussed in section III below. Our experimental data are also in good agreement with these theoretical predictions within a 5 % difference at the smaller c.m. angles.

III. DATA ANALYSIS AND RESULTS

The angular distribution of the $d(^{11}C,^{12}N)n$ reaction was obtained from the measured ^{12}N peaks and is shown in Fig. 5. Although the experimental setup was designed to cover emitted ^{12}N nuclei from 10.9° to 171.4° c.m., the data at angles beyond 72° c.m. had to be excluded because of their poor statistics (e.g., see Fig. 3). The experimental angular distribution was then compared with theoretical predictions to extract the ANC from the transfer reaction data, and the $^{12}N \rightarrow {}^{11}C+p$ ANC was deduced from the following equation (see Ref. [Li03, Ta03])

$$\left(\frac{d\sigma}{d\Omega}\right)_{\exp} = \left(\frac{C^d}{b^d}\right)^2 \times \left[\left(\frac{C^{^{12}N}_{p1/2}}{b^{^{12}N}_{p1/2}}\right)^2 \times \left(\frac{d\sigma_{p1/2}}{d\Omega}\right)_{DWBA} + \left(\frac{C^{^{12}N}_{p3/2}}{b^{^{12}N}_{p3/2}}\right)^2 \times \left(\frac{d\sigma_{p3/2}}{d\Omega}\right)_{DWBA}\right]$$

$$= \left(\frac{C^d}{b^d}\right)^2 \times \left(C^{^{12}N}_{p1/2}\right)^2 \times \left[\frac{\left(\frac{d\sigma_{p1/2}}{d\Omega}\right)_{DWBA}}{\left(b^{^{12}N}_{p1/2}\right)^2} + \left(\frac{C^{^{12}N}_{p3/2}}{C^{^{12}N}_{p1/2}}\right)^2 \times \frac{\left(\frac{d\sigma_{p3/2}}{d\Omega}\right)_{DWBA}}{\left(b^{^{12}N}_{p3/2}\right)^2}\right], \quad (1)$$

where C_{lj} and b_{lj} represent the asymptotic normalization coefficient and single particle ANC of the transferred proton with orbital angular momentum l and total angular momentum j, respectively. For the DWBA calculation, three sets of global optical model parameters for the d(^{11}C,^{12}N)n reaction were obtained from the literature [Wa69, Ha71, Da80] (since ^{11}C optical model parameters were not available). These parameter sets for the d(^{11}C,^{12}N)n reaction are given in Table I (Parameter Set III differs from Set I only by its spin-orbit potentials.)

The DWBA analysis with these parameter sets was first tested with our d(^{12}C,^{13}N)n data (with the parameter sets appropriately adjusted). The calculated d(^{12}C,^{13}N)n angular distributions shown in Fig. 4 are in good agreement with our experimental results, and the ^{12}C(d,n)^{13}N study [Ka86]. The angular distributions that resulted from these parameter sets start to diverge as the c.m. angle increases, but the differences at smaller angles remained less than 3% (see Fig. 4). For the optical model parameter sets, the adiabatic approximation method was also taken into account in order to include the break-up effect of the loosely bound deuteron [Ha71, Jo72, Ka86].

Then, these parameter sets were used to calculate $\left(\frac{d\sigma_{p1/2}}{d\Omega}\right)_{DWBA}$ and $\left(\frac{d\sigma_{p3/2}}{d\Omega}\right)_{DWBA}$ using the zero-range DWUCK4 code with a reaction normalization coefficient of $D_o^2 = 1.55\times10^4\, MeV\cdot fm^3$ [Sa83, Ku93, Im01]. The ANC of $d \to p + n$, $(C^d)^2$ is known to be 0.76 fm^{-1} [Bl77], and the ratio of $\left(C^{^{12}N}_{p3/2}\right)^2$ to $\left(C^{^{12}N}_{p1/2}\right)^2$ is 0.17, which is obtained from an average value in a recent shell model calculation [Ti03a].

Given all this available information, the averaged DWBA cross section from three different optical model parameter sets is then compared to the experimental result, adjusting $C_{p_{1/2}}^{^{12}N}$ as a fitting parameter. Figure 5 shows that the overall shape of the DWBA cross section successfully describes the experimental result at forward angles. The extracted ANC is found to be $\left(C_{p_{1/2}}^{^{12}N}\right)^2 = 1.56 \pm 0.23\, fm^{-1}$, and the ratio of $p_{1/2}$ to $p_{3/2}$ leads to $\left(C_{p_{3/2}}^{^{12}N}\right)^2 = 0.26 \pm 0.05\, fm^{-1}$. Finally, the total effective ^{12}N$\rightarrow^{11}$C+p ANC is obtained to be $\left(C_{eff}^{^{12}N}\right)^2 = \left(C_{p_{1/2}}^{^{12}N}\right)^2 + \left(C_{p_{3/2}}^{^{12}N}\right)^2 = 1.83 \pm 0.27\, fm^{-1}$. The uncertainty mainly comes from the statistical error (11.0%) in the experiment and the deviation of theoretical DWBA cross section (3.2%) caused by different optical potential parameter sets.

The extracted ANC is then used to calculate the direct capture cross section to the ^{12}N ground state using the RADCAP code [Be03], and the Breit-Wigner resonance formula is used for the proton capture through the 2^+ (E_x=0.960 MeV) and 2^- (E_x=1.190 MeV) resonance states in ^{12}N. For the 2^+ state, only an upper limit of 20 keV has been established for the Γ_p [Aj90], and suggested values of 5.5 keV [Le95] and 2.6 meV [Wi89, Le95] have been used for Γ_p and Γ_γ, respectively. A Γ_p of 118 keV [Aj90] and Γ_γ of 13.0 meV [Mi02] were adopted for the 2^- state. The total capture cross section $\sigma(E)$ is then obtained by summing direct and resonant capture cross sections, including taking into account an interference term between the direct capture and the broad 2^- resonance state [Ro74].

The astrophysical S-factor is calculated through a relation given by

$$S(E) = E\sigma(E)\exp(2\pi\eta), \tag{2}$$

where η is the Sommerfeld parameter. Fig. 6 shows the calculated astrophysical S-factor, and the extrapolated S-factor at zero energy is found to be $S(0) = 0.097 \pm 0.020$ keV b in this work. Given the astrophysical S-factor, the ^{11}C(p,γ) reaction rate as a function of stellar temperature can also be calculated by

$$N_A < \sigma v >= N_A \left(\frac{8}{\pi \mu} \right)^{1/2} \left(\frac{1}{kT} \right)^{3/2} \int_0^\infty S(E) \exp\left[-\frac{E_G^{1/2}}{E^{1/2}} - \frac{E}{kT} \right] dE \,, \qquad (3)$$

where N_A is Avogadro's number and E_G is the Gammow energy [Ro88]. The calculated ^{11}C(p,γ) reaction rate is shown in Fig. 7, and this figure clearly shows that the sum of the direct capture and the resonant capture through the 2^- state dominates in the low temperature region.

IV. DISCUSSION AND SUMMARY

The extracted ^{12}N$\rightarrow^{11}$C+p ANC of $1.83 \pm 0.27\, fm^{-1}$ in this work is less than the $2.86 \pm 0.91\, fm^{-1}$ from the same transfer reaction study of Ref. [Li03] (but the measurements agree within error bars). However, our result is improved by its better statistics (due to our higher ^{11}C beam intensity), and shows good agreement with the reported value of $\left(C_{eff}^{^{12}N}\right)^2 = 1.73 \pm 0.25\, fm^{-1}$ from the ^{14}N(^{11}C,^{12}N)^{13}C reaction [Ta03]. This shows that the ANC can be experimentally obtained with consistent nuclear properties regardless of the experimental reaction scheme. In addition, a study [Ti03b] has reported that the ^{12}N ANC could be estimated based on known information for its mirror nucleus, ^{12}B. They developed a relationship between the proton and neutron squared ANC's in the two mirror nuclei, and then obtained a ratio of 1.37 between ^{12}N and ^{12}B from theoretical potential model calculations. The experimental ^{12}B ANC is

$\left(C_{\exp}^{^{12}B}\right)^2 = \left(C_{n1/2}^{^{12}B}\right)^2 + \left(C_{n3/2}^{^{12}B}\right)^2 = 1.35\,fm^{-1}$ from a d(^{11}B,^{12}B)p reaction study [Li01]. This implies that the effective ^{12}N ANC value is expected to be $1.84\,fm^{-1}$, which is in accordance with our experimental result. Recently, another d(^{11}B,^{12}B)p study also reported $\left(C_{eff}^{^{12}N}\right)^2 = 1.63 \pm 0.35\,fm^{-1}$, using a ratio of $\frac{\left(C_{eff}^{^{12}N}\right)^2}{\left(C_{eff}^{^{12}B}\right)^2} = 1.36 \pm 0.03$ and the extracted ^{12}B ANC value of $\left(C_{eff}^{^{12}B}\right)^2 = 1.20 \pm 0.26\,fm^{-1}$ [Gu07].

The astrophysical S-factor at zero energy, $S(0)$, from our experiment turned out to be about two times larger than that from the Coulomb breakup experiment [Le95], but agrees with those from ANC method studies. The direct capture reaction dominantly contributes to the total S-factor in the energy region of astrophysical interest; the interference term increased the S-factor slightly in the low energy region as shown in Fig. 6.

In the temperature region from $0.2 < T_9 < 0.4$, the reaction rate is dominated by the direct and the 2^- resonance captures, while the contribution from the 2^+ state is less important (see Fig. 7). As a result, we can confirm a) that the major contribution to the ^{11}C(p, γ) reaction rate comes from the direct capture reaction as was concluded in previous studies, and b) that the ^{11}C(p, γ) reaction rate appears to be higher than the previous Coulomb breakup estimate [Le95]. This result supports the idea that the ^{7}Be(α,γ)^{11}C(p, γ)^{12}N($e^+\nu$)^{12}C reaction sequence is one of the alternative paths in producing CNO nuclei in low-metallicity supermassive stars.

ACKNOWLEDGMENTS

This work was supported by the U.S. Department of Energy, Office of Nuclear Physics, under contract No. DE-AC03-76SF00098. We thank Prof. David K. Geiger of the State University of New York at Geneseo for providing the CD_2 target.

REFERENCES

[Fu86] G. M. Fuller, S. E. Woosley, and T. A. Weaver., Astrophys. J. 307, 675 (1986).

[Wi89] M. Wiescher et al., Astrophys. J. 343, 352 (1998).

[Le95] A. Lefebvre et al., Nucl. Phys. A592, 69 (1995).

[Mu01] A. M. Mukhamedzhanov et al., Phys. Rev. C 63, 024612 (2001).

[Ga02] C. A. Gagliardi et al., Eur. Phys. J. A 13, 227 (2002).

[Mu06] A. M. Mukhamedzhanov et al., Eur. Phys. J. A 27, 205 (2006).

[Ta03] X. Tang et al., Phys. Rev. C 67, 015804 (2003).

[Li03] W. Liu et al., Nucl. Phys. A728, 275 (2003).

[Gu05] F. Q. Guo et al., Phys. Rev. C 72, 034312 (2005).

[Jo00] R. Joosten et al., Phys. Rev. Lett. 84, 5066 (2000).

[Le07] D. W. Lee et al., Phys. Rev. C 76, 024314 (2007).

[Po00] J. Powell et al., Nucl. Instrum. Methods Phys. Res. A 455, 452 (2000).

[Po03] J. Powell et al., Nucl. Instrum. Methods Phys. Res. B 204, 440 (2003).

[Wa69] B. A. Watson et al., Phys. Rev. 182, 977 (1969).

[Ha71] J. D. Harvey, and R. C. Johnson, Phys. Rev. C 3, 636 (1971).

[Da80] W. W. Daehnick et al., Phys. Rev. C 21, 2253 (1980).

[Ku93] P. D. Kunz, computer code DWUCK4, University of Colorado (unpublished), (1993).

[Ka86] T. Kawamura et al., Cyclotron and Radioisotope Center, Tohoku University, Annual Report 1986, 10 (1986).

[Jo72] R. C. Johnson and P. J. R. Soper, Nucl. Phys. A182, 619 (1972).

[Sa83] G. R. Satchler, Direct Nuclear Reactions, Oxford University Press, Oxford OX2 6DP (1983).

[Im01] N. Imai et al., Nucl. Phys. A688, 281c (2001).

[Bl77] L. D. Blokhintsev, I. Borbely, and E. I. Dolinskii, Sov. J. Part. Nucl. 8, 485 (1977).

[Ti03a] N. K. Timofeyuk and S. B. Igamov, Nucl. Phys. A713, 217 (2003).

[Be03] C. A. Bertulani, Comput. Phys. Commun. 156, 123 (2003).

[Aj90] F. Ajzenberg-Selove, Nucl. Phys. A506, 1 (1990).

[Mi02] T. Minemura et al., RIKEN Accel. Prog. Rep. A35, (2002).

[Ro74] C. Rolfs and R. E. Azuma, Nucl. Phys. A227, 291 (1974).

[Ro88] C. Rolfs and W. Rodney, Cauldrons in the Cosmos (University of Chicago Press, Chicago, 1988).

[Ti03b] N. K. Timofeyuk, R. C. Johnson and A. M. Mukhamedzhanov, Phys. Rev. Lett. 91, 232501 (2003).

[Li01] Z. H. Liu et al., Phys. Rev. C 64, 034312 (2001).

[Gu07] B. Guo et al., J. Phys. G 34, 103 (2007).

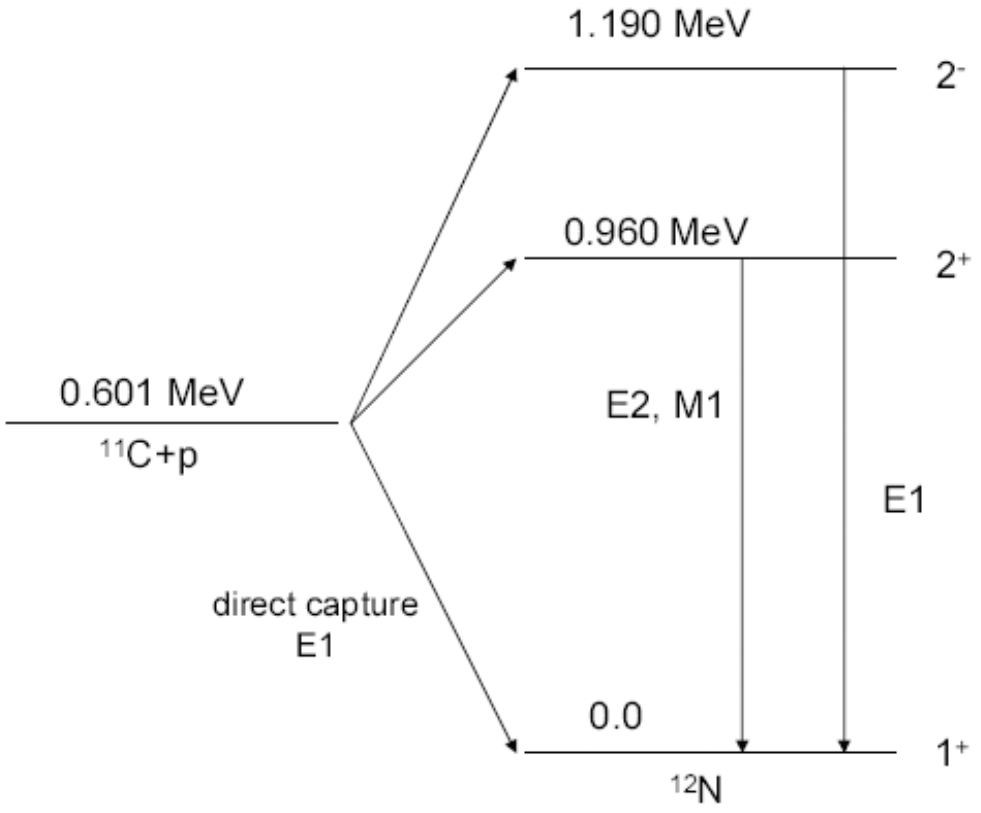

FIG. 1. The $^{11}C(p,\gamma)$ radiative capture reaction scheme. Resonant captures through the 2^+ and 2^- states in ^{12}N are also shown along with direct capture to the $^{12}N_{g.s.}$ Note that all excited states in ^{12}N are proton unbound.

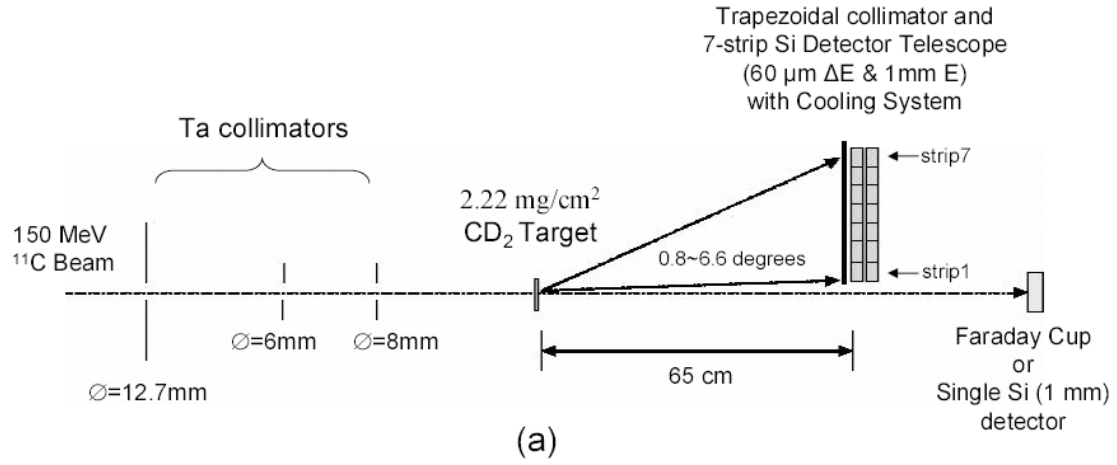

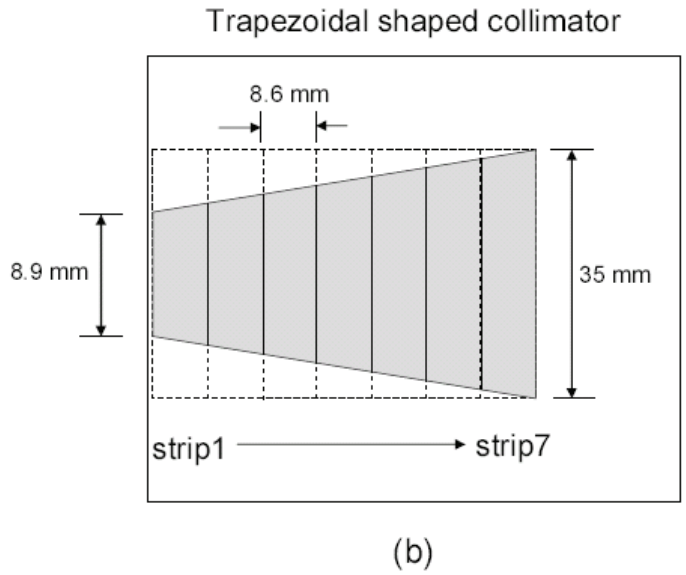

FIG. 2. (a) The d(^{11}C,^{12}N)n reaction experimental setup. (b) Front view of the 7-strip Si ΔE detector through a trapezoidal collimator.

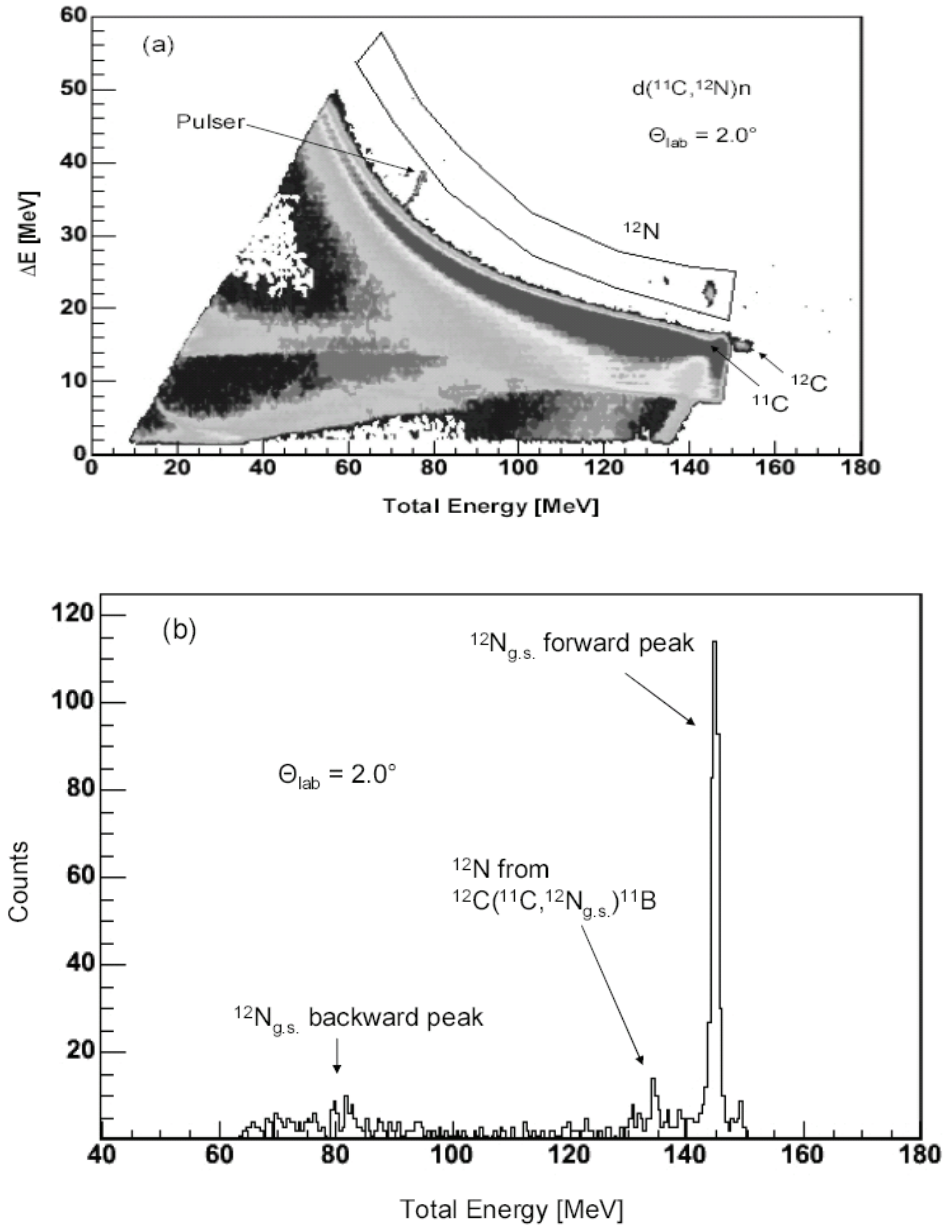

FIG. 3. (a) A two-dimensional particle identification spectrum from ΔE-E coincidences at the second strip plotted as ΔE vs. Total Energy (=ΔE+E). The ^{12}N gate is shown above the scattered ^{11}C beam. Note that ^{12}C also appears from the d(^{11}C,^{12}C)p reaction. (b) A one-dimensional spectrum inside the ^{12}N gate. A $^{12}N_{g.s.}$ forward peak is clearly observed along with background from the $^{12}C(^{11}C,^{12}N_{g.s.})^{11}B$ reaction. The expected position of the $^{12}N_{g.s.}$ backward peak is also indicated.

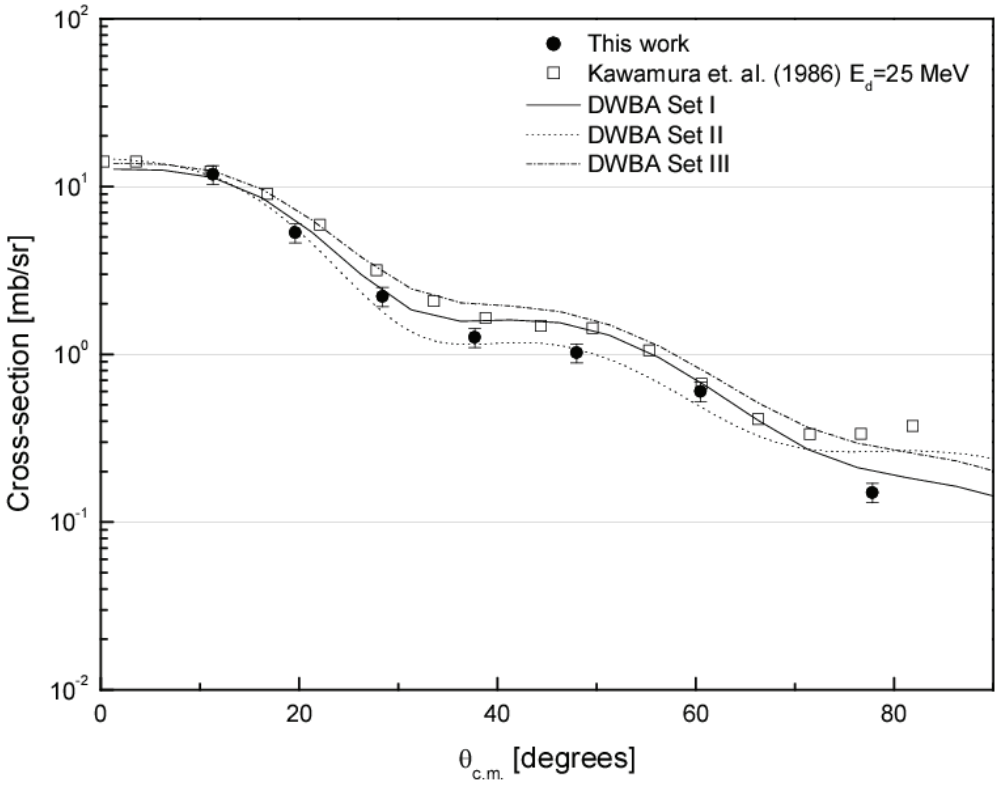

FIG. 4. The d(^{12}C,^{13}N)n reaction angular distribution. Our experimental results are compared to those from a previous study of ^{12}C(d,n)^{13}N (see text). Error bars are shown (this work) or are within the open squares. Three different theoretical angular distributions (DWBA) are also shown.

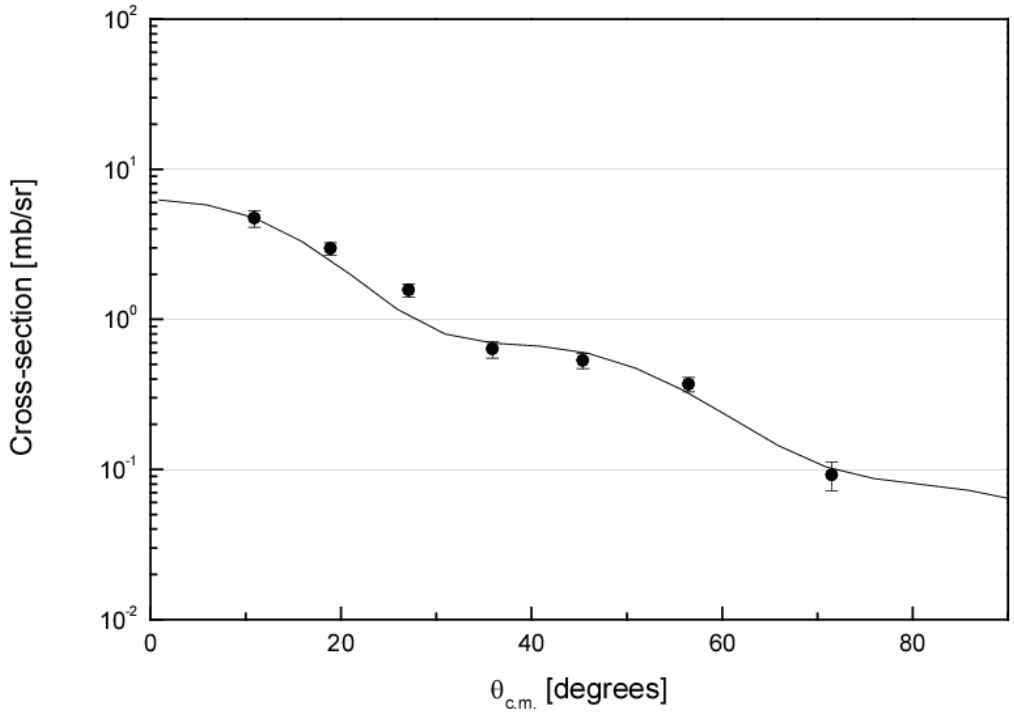

FIG. 5. The d(^{11}C,^{12}N)n reaction angular distribution. Black circles are our experimental results, and the solid line represents theoretical DWBA cross sections based on three different optical model parameter sets (see text).

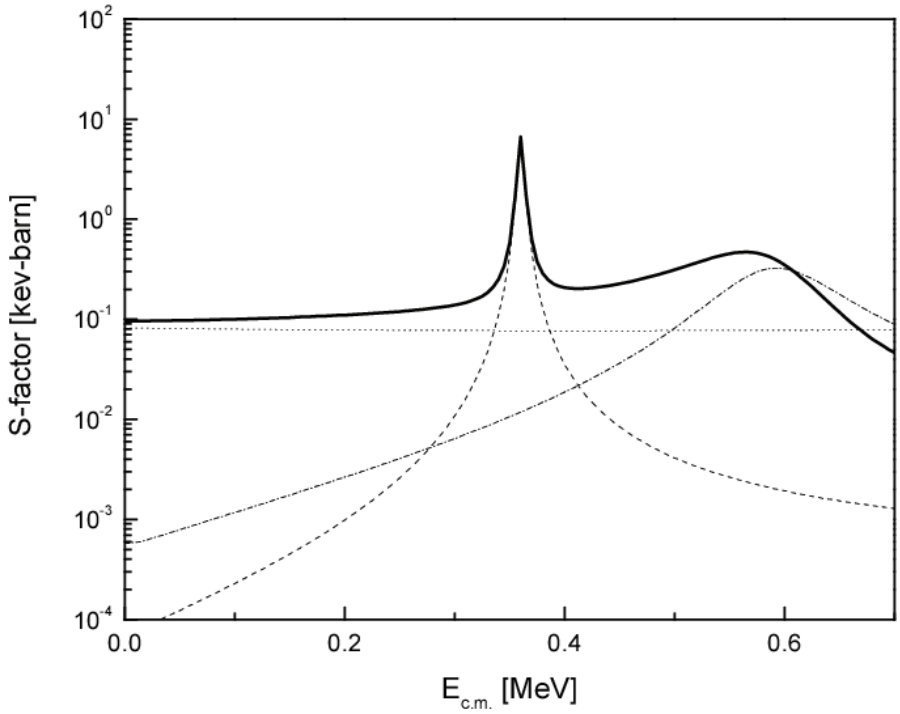

FIG. 6. The calculated $^{11}C(p,\gamma)$ astrophysical S-factor, based on the extracted ANC value. The dotted line represents the S-factor from direct capture. The dashed line is the contribution from the 2^{+} state, and the dash-dotted line is from the 2^{-} state in ^{12}N. The solid line is the total S-factor, including the interference term between direct capture and the 2^{-} state.

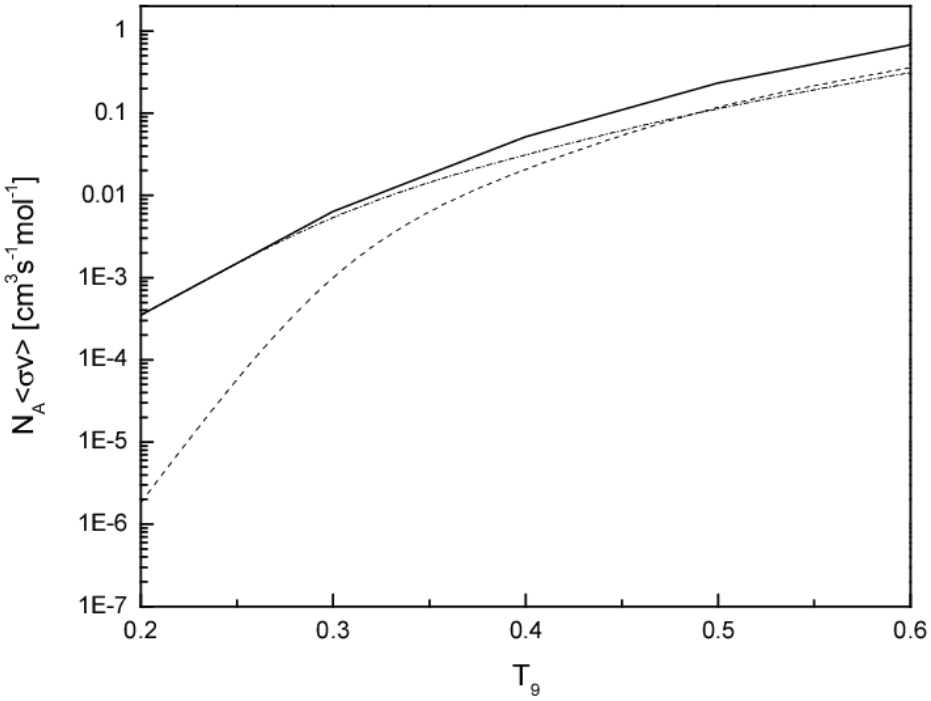

FIG. 7. $^{11}C(p,\gamma)$ stellar reaction rate. The dashed line shows the contribution of the narrow 2^+ state, and the dash-dotted line is the combination of the direct capture and the broad 2^- state. The solid line represents the total $^{11}C(p,\gamma)$ stellar reaction rate as a function of stellar temperature T_9 (10^9 K). See text.

Table I. Optical model parameters for the d(^{11}C,^{12}N)n reaction. (V and W are expressed in MeV, and r and a in *fm.*)[§].

Set		V_r	W_i	W_D	V_{so}	r_o	a_o	r_i	a_i	r_{so}	a_{so}	r_c
I :	d [a,b]	114.2	0.0	13.68	3.0	1.14	0.61	1.14	0.54	1.14	0.61	1.14
	n [a]	58.1	0.0	9.98	26.0	1.13	0.57	1.13	0.50	1.13	0.57	1.13
II :	d [c]	83.8	0.93	11.98	6.54	1.17	0.76	1.33	0.53	1.07	0.66	1.30
	n [a]	58.1	0.0	9.98	11.0	1.13	0.57	1.13	0.50	1.13	0.57	1.13
III :	d [a,b]	114.2	0.0	13.68	11.0	1.14	0.61	1.14	0.54	1.14	0.61	1.14
	n [a]	58.1	0.0	9.98	11.0	1.13	0.57	1.13	0.50	1.13	0.57	1.13

a. From Ref. [Wa69]

b. From Ref. [Ha71]

c. From Ref. [Da80]

[§] The potential $V(r)$ in the DWUCK4 code [Ku93] is given by

$$V(r) = -V_r f(r, r_o, a_o) - iW_i f(r, r_i, a_i) + 4iW_D \frac{d}{dr} f(r, r_i, a_i)$$
$$+ V_{so}\left(\frac{\hbar}{m_\pi c}\right)\frac{1}{r}\frac{d}{dr} f(r, r_{so}, a_{so})\mathbf{L}\cdot\mathbf{s} + V_c(r_c) \quad ,$$

where $f(r, r_j, a_j) = \dfrac{1}{1+\exp\left(\dfrac{r - r_j M_{\text{target}}^{1/3}}{a_j}\right)}$ and $V_c(r_c)$ is the Coulomb potential.